AIAA SciTech
13-17 January 2014, National Harbor, Maryland
32nd ASME Wind Energy Symposium

Experimental quantification of the entrainment of kinetic energy and production of turbulence in the wake of a wind turbine with Particle Image Velocimetry

L.E.M. Lignarolo[1], D. Ragni[1], C.J. Simão Ferreira[1], G.J.W. van Bussel[1]
[1]*Delft University of Technology, Aerodynamics Wind Energy Flight Performance and Propulsion, Delft, 2629HS, The Netherlands*

The role of the tip-vortex pairwise instability ("leapfrogging") is investigated in relation to the process of kinetic energy transport and turbulence production within the shear layer of a horizontal-axis wind-turbine wake. Experiments are conducted in an open-jet wind-tunnel on a wind turbine model. Stereoscopic particle image velocimetry (SPIV) is employed to obtain the velocity field in a meridian plane encompassing a large portion of the wake past the rotor model. Measurements with both phase-locked and unconditioned sampling techniques allow for a triple decomposition of the flow fields. The levels of turbulence intensity show a dominant role of random fluctuations after the location of the pairwise instability. Computation of the kinetic energy fluxes across the wake shear layer shows the presence of three main zones. Prior to the onset of the instability, vortices shed from the blade inhibit the turbulent mixing of the wake during its expansion. The region affected by leapfrogging exhibits a sudden increase of the net entrainment of kinetic energy. Downstream, the energy exchange is characterized by a pronounced turbulent mixing, only due to random turbulent motions. Leapfrogging determines the end of the wake expansion and with the onset of a more pronounced turbulent mixing, coincident with the beginning of the wake re-energising process.

Nomenclature

α	angle of attack
λ	tip-speed ratio
ρ	density
φ	phase
ω	vorticity
Γ	circulation
a	induction factor
c	blade chord
c_p	pressure coefficient
p	pressure
r	blade radial location
t	time
x,y,z	axial, radial and azimuthal direction
u_i	velocity
u_{RMS}	RMS velocity
$\langle u_{s,i} u_{s,j} \rangle$	Reynolds stresses in the phase-lock field
$\overline{u'_i u'_j}$	Reynolds stresses in the unconditioned average field

C_t	thrust coefficient
C_l	lift coefficient
D	diameter
H	enthalpy
R	radius
Re	Reynolds number
TI	turbulence intensity
U_∞	free stream velocity
$\overline{\ }$	unconditioned average quantity
$\langle\ \rangle$	phase-lock average velocity

I. Introduction

THE turbulent flow in the wake of a rotor is relevant for many engineering applications, ranging from wind-turbines to marine propellers and helicopters. When considering clusters or arrays of rotor as in wind farms [25], the persistence of the wake over a significant distance reduces the energy performance of the entire farm, and induces unsteady loads, noise and fatigue on the downwind rotors [29, 24]. Wake effects increase in off-shore wind farms, where the turbulence intensity is lower than on-shore and wakes persist for several diameters due to the reduced atmospheric turbulence [14]. In offshore wind turbines, knowledge about the basic mechanisms behind the breakdown of the tip-vortices spiral system is needed to estimate the extension of the near wake region, where strong coherent fluctuations dominate. Moreover, the instability and breakdown of the helical system of vortices in the near wake has strong repercussions on the development of the turbulence in the far wake, where the mixing process between the inner wake and the outer free-stream is carried out. Anticipating the mixing process and the recovery of the momentum losses could lower the cost of energy by decreasing the spacing between turbines.

The stability properties of the helical system of vortex filaments in the wake of a rotor have been investigated by several authors (see the reviews by Ref. 28). Previous research in wake stability analysis showed that, in the near-wake, the vortical structures released by the blade tip and root mutually interact [21]; this interaction maintains the tip-vortices in their stable helical pattern, which is otherwise unstable regardless of the characteristics of the vorticity distribution [31], as already analytically demonstrated by Ref. 15. Most of the research on the stability of vortical structures is valid for a wide range of circulation values (see Ref. 10), therefore applicable in both helicopters [16], wind-turbines [20], naval propellers [10] and aircraft propellers applications. Notwithstanding the amount of studies associated with the stability of the wake in the near field, the identification of the triggering mechanism in the transition to the far field [10] is still an open problem in fluid-dynamics, especially with the presence of consistent viscosity and turbulence.

The effect of this near-wake instability on the mixing process of the wind turbine far wake has only been addressed by Ref. 18, who ascribes the absence of energy recovery in the near wake to the *shielding* effect of the tip vortices; this contradicts previous literature, where the tip vortices were regarded as structures enhancing the mixing by entraining high-momentum fluid from the outer stream [12]. However, many studies about the role of coherent structures and the effects of vortex pairwise instability on the energy and momentum transfer in bluff body wakes, jets and mixing layers are available in literature. Ref. 2, Ref. 3, Ref. 32, Ref. 5 showed that the vortex pairing promotes transport of transverse momentum across shear layers. The wake of a wind turbine is characterized by the presence of vortices which have a very different origin although behaving very similarly to the one of a mixing layer or planar jet (see Ref. 19 for theoretical, Ref. 13 for numerical, and Ref. 10 for experimental analysis) as it will be also shown in the present paper.

A common approach for the simulation of wind farms is to model the rotor as an actuator disk; this approach misestimates the effects of flow turbulence[4] and disregards the effects of the tip-vortex helix instability. Consequently the mixing process across the wake interface and ultimately the rate at which the wake recovers momentum is incorrectly modelled. Ref. 24 explains how the strong velocity gradients introduced at the wake edges in the actuator disc model are not physical and cause unrealistic turbulence sources enhancing the wake dissipation, especially with the use of common turbulence models (as the k-ε model) and suggested to not use the actuator disc model for wind farms simulations with turbine spacing smaller than five diameters. Ref. 33 performed a comparison between wind tunnel measurements of a wind turbine wake and numerical simulations using the actuator disc model both with and without wake rotation. Experiments and numerical results showed discrepancies till the far wake as far as the turbulence intensity evolution is concerned, while a better agreement in the evolution of the wake velocity profile was found.

The present investigation focuses on the experimental analysis of the physics governing the mixing process in the shear layer of a wind-turbine wake, showing how the high kinetic energy of the free-stream is entrained in the inner regions of the wake, leading to its re-energising. The experiments are conducted in a closed-loop open-jet facility of the Delft University of Technology (TUDelft) where a scaled model of a two-bladed wind-turbine is installed. The analysis of the wake flow is conducted by mean of stereoscopic particle image velocimetry SPIV, [22]. Previous works by Ref. 8, Ref. 27 and Ref. 30 have already demonstrated the accuracy and reliability of this measurement technique when dealing with rotor wakes. In the present study, the measurements are acquired along axial planes past the rotor till 5 diameters downstream (in this paper only the instability region up to ~3 diameters downstream will be investigated). The ability to measure both unconditioned averaged flow field properties as well as phase-locked snapshots allows to uncover the details of the energy transport following a triple decomposition of the velocity field into mean, periodic and random fluctuating components [23].

II. Method

A. Kinetic energy transport and triple decomposition

Due to the presence of periodic vortical structures in the flow, the kinetic energy transport is studied via a triple decomposition of the flow with mean, periodic and turbulent velocity fields [23, 3, 1]. The procedure is typically applied in mixing flows, [9] when the unsteady boundary conditions are of periodic type (rotors, flapping aerofoils, etc.) to separate the contribution of the periodic fluctuations from the random turbulence. The triple decomposition defines the velocity field u_i and the pressure field p_i as:

$$\begin{aligned} u_i(t) &= \overline{u_i} + \widetilde{u_i}(t+nT) + u_{s,i}(t) \\ p(t) &= \bar{p} + \tilde{p}(t+nT) + p_s(t) \end{aligned} \tag{1}$$

where u_i is the instantaneous velocity field, $\overline{u_i}$ denotes the time average velocity field, $\widetilde{u_i}$ the periodic fluctuations and the $u_{s,i}$ indicates the randomly fluctuating velocity component. In the classical Reynolds decomposition, the velocity field is $u_i = \overline{u_i} + u'$, where $u' = \widetilde{u_i} + u_{s,i}$. Typically, the time average flow $\overline{u_i}$ is obtained as ensemble average of a series of unconditioned samples, while the phase-average field $\langle u_i \rangle$ is obtained by phase-locking the measurement acquisition with the periodic motion,. The fluctuating component pertaining to one phase can be obtained from the phase-locked average field as

$$\widetilde{u_i} = \langle u_i \rangle - \overline{u_i} \tag{2}$$

for each phase. This entails a clear distinction between the ensemble and phase-averaged Reynolds stresses as:

$$\overline{u'_i u'_j} = \sqrt{\frac{\sum_{k=1}^{N}[u_i(t_k)-\overline{u_i}][u_j(t_k)-\overline{u_j}]}{N}}; \qquad \langle u_{s,i}u_{s,j}\rangle_\varphi = \sqrt{\frac{\sum_{k=1}^{N}[u_i(t_{k,\varphi})-\langle u_i\rangle][u_j(t_{k\varphi,})-\langle u_j\rangle]}{N}} \tag{3}$$

The mathematical relationship between the two quantities is:

$$\overline{u'_i u'_j} = \overline{\widetilde{u_i}\widetilde{u_j}} + \overline{u_{s,i}u_{s,j}} \tag{4}$$

Where:

$$\overline{u_{s,i}u_{s,j}} = \sum_{\varphi=1}^{N_f} \frac{\langle u_{s,i}u_{s,j}\rangle_\varphi}{N_f}; \qquad \overline{\widetilde{u_i}\widetilde{u_j}} = \sum_{\varphi=1}^{N_f} \frac{\widetilde{u_i}\widetilde{u_j}_\varphi}{N_f}; \tag{5}$$

is the average over all phases of the Reynolds stresses relative to the random fluctuations and periodic motions respectively. As denoted by Ref. 23 the average kinetic energy associated with the fluid having velocity u_i is:

$$\frac{1}{2}\overline{u_i u_i} = \frac{1}{2}\overline{u_i}\,\overline{u_i} + \frac{1}{2}\overline{\widetilde{u_i}\widetilde{u_i}} + \frac{1}{2}\overline{u_{s,i}u_{s,i}} = K_E + K_p + K_T \tag{6}$$

where K_E is the kinetic energy of the mean flow, K_P of the periodic structures and K_T is the contribution of the random turbulent fluctuations . Neglecting the viscous effects, the transport equation of the mean flow kinetic energy for one phases φ in the phase-locked form as derived from Ref. 23 by multiplying the Navier-Stokes by $\overline{u_i}$ and time averaging reads as:

$$\left(\overline{u_j}+\widetilde{u_j}\right)\frac{\partial K_E}{\partial x_j}=-\left(\frac{\partial \bar{p}\overline{u_i}}{\partial x_i}+\frac{\partial \tilde{p}\overline{u_i}}{\partial x_i}\right)-\overline{u_i}\left(\frac{\partial \widetilde{u_i}}{\partial t}+\overline{u_j}\frac{\partial \widetilde{u_i}}{\partial x_j}\right)-\left(-\langle u_{s,i}u_{s,j}\rangle-\widetilde{u_i}\widetilde{u_j}\right)\frac{\partial \overline{u_i}}{\partial x_j}$$
$$-\frac{\partial}{\partial x_j}\left[\overline{u_i}\langle u_{s,i}u_{s,j}\rangle+\overline{u_i}\left(\widetilde{u_i}\widetilde{u_j}\right)\right] \tag{7}$$

The term on the left-hand side denotes the net rate of increase of the energy component, while the right-hand describes the mechanisms governing it. The first and fourth terms on the right represent the transport of mean flow kinetic energy within the flow by means of the pressure gradient, periodic and random flow fluctuations. The second term derives from the fact that the obtained averaged field is convected with the mean flow. The third term represents the mean flow kinetic energy which is adsorbed by the periodic and random flow fluctuations. Eq. (7) allows restricting the study to one single phase, with evident advantages in terms of duration of experiments. The present manuscript will focus on the third and the fourth term of the right-hand side of Eq. (7), representing respectively the mean flow kinetic energy loss into turbulence and coherent vortices and the kinetic energy transport due to the turbulence and the periodic vortices at the phase φ.

B. Experimental set-up and test conditions

Detailed information about the wind tunnel, the wind turbine model design and characteristics and about the stereo PIV setup can be found in Ref. 17. In this section, only the most important information are reported.

- **Wind tunnel and wind turbine model**

Experiments have been conducted in the low-speed closed-loop open-jet wind tunnel located at the Aerodynamics Department of the Delft University of Technology. The wind tunnel, with its octagonal test section has an equivalent diameter of 3 m and a contraction ratio of 3:1, delivering a uniform stream with approximately 0.5% turbulent intensity up to 1 m from the nozzle and lower than 2% at 6 m from the nozzle exit. At the latter distance, the uniform flow region reduces to approximately 2x2 m2.

The employed model is a two-bladed horizontal-axis wind-turbine shown in

Figure 1, with design tip speed ratio λ = 6 and a rotor diameter D = 0.6 m. The wind-tunnel blockage-ratio is 0.04. An Eppler E387 [26] airfoil with a thickness to chord ratio of 9.06% is used along the blade span. The airfoil is particularly suited for low Reynolds numbers. Blades have been especially design for constant bound circulation along the span at the design tip-speed ratio. The chord-based Reynolds number at the tip region is approximately Re=100,000 at λ = 6. The nacelle has a diameter of 0.038 m (6.3% of the rotor diameter) and contains an optical trigger (opto-coupler TCST 2103) which provides a one pulse per revolution signal allowing for the PIV phase synchronization for phase-locked measurments.

Parameters		**Units SI**	$C_{t,1}$	$C_{t,2}$
Free-stream velocity	U_∞	[m/s]	3.8	5.7
Rotational frequency	ω	[rad/s]	60.8	113.1
Thrust coefficient	C_t	-	0.82	0.89
Tip speed ratio	λ	-	4.8	6

Table 1. Test conditions for the two investigated thrust coefficients.

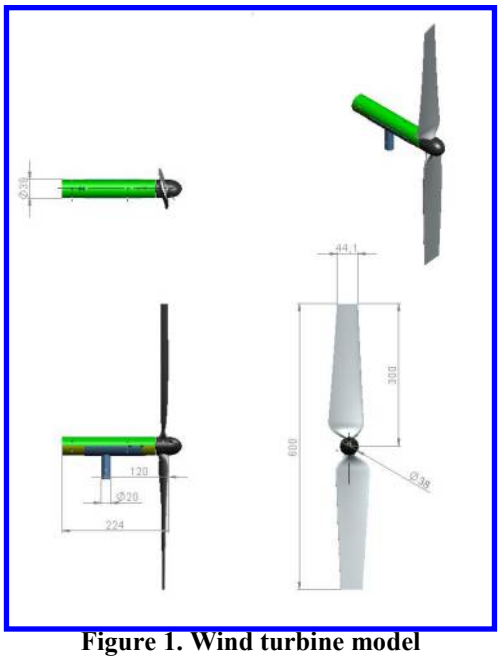

Figure 1. Wind turbine model

- **Stereoscopic particle image velocimetry**

Experimental data are obtained through stereoscopic particle image velocimetry, which provides three-component velocity fields on a plane and processed by average of correlation maps, as detailed in Table 2. A stereoscopic PIV setup has been installed in a traversing system able to scan the flow field in the wake of the horizontal-axis wind-turbine wake. The required illumination is provided by a Quantel Evergreen Nd:YAG laser system with 200 mJ/pulse. Two LaVision Imager Pro LX 16 Mpix (4870 × 3246 px2, 12 bits) with pixel pitch of 7.4 μm/px are used to image a field of view of 0.357 × 0.253 m2. Seeding was provided in the test section by a SAFEX smoke generator with SAFEX MIX, able to produce liquid droplets of less than 1 μm. The entire setup was mounted on a traversing system able to translate in two directions. Ensemble of 400 (phase-locked), 720 (unconditioned) double-frame recordings have been acquired and processed by LaVision Davis 8.1.4. Interrogation windows of 24 × 24 px2 with 50% overlap allows to have a vector resolution of 1.76 mm, and a vector pitch of 0.88 mm.

Parameters		**Stereoscopic PIV setup**	
Measurement field of view	FOV	357 mm × 253 mm	4870 px × 3246 px
Measurement resolution	Iw	1.76 mm × 1.76 mm	24 px × 24 px
Digital resolution	DR	13.64 px/mm	
Magnification factor	M	0.10	
Vectors	N#	404 × 270	

Table 2. System parameters for the stereoscopic PIV setup

III. Results and discussion

C. Analysis of the flow topology and vortex evolution

- **Wake velocity field**

The velocity field in the wake up to 3 diameters downstream is reconstructed by combining the different fields of view from the PIV measurements. In Figure 2, the ensemble averaged axial velocity (*x*-direction) spatial distribution is presented for the two different values of the thrust coefficient, respectively 0.82 and 0.89 (

Table **1**). The onset of the wake instability is represented by a localised shear layer thickness increase developing in proximity of the maximum wake expansion, respectively starting at $x/D \sim 1.3$ for $\lambda = 4.8$ and $x/D \sim 1$ for $\lambda = 6$. The maximum thickness of the shear layer coincides with the location where the tip-vortices had paired in doublets and completed a 90° rotation (see Figure 4). As already noted by Ref. 10, the onset of the wake instability depends upon the tip-speed ratio, with higher tip-speed ratio causing an earlier instability. This is due to the shorter pitch of the helical vortex filament, which leads to a more rapid onset of interaction between vortices.

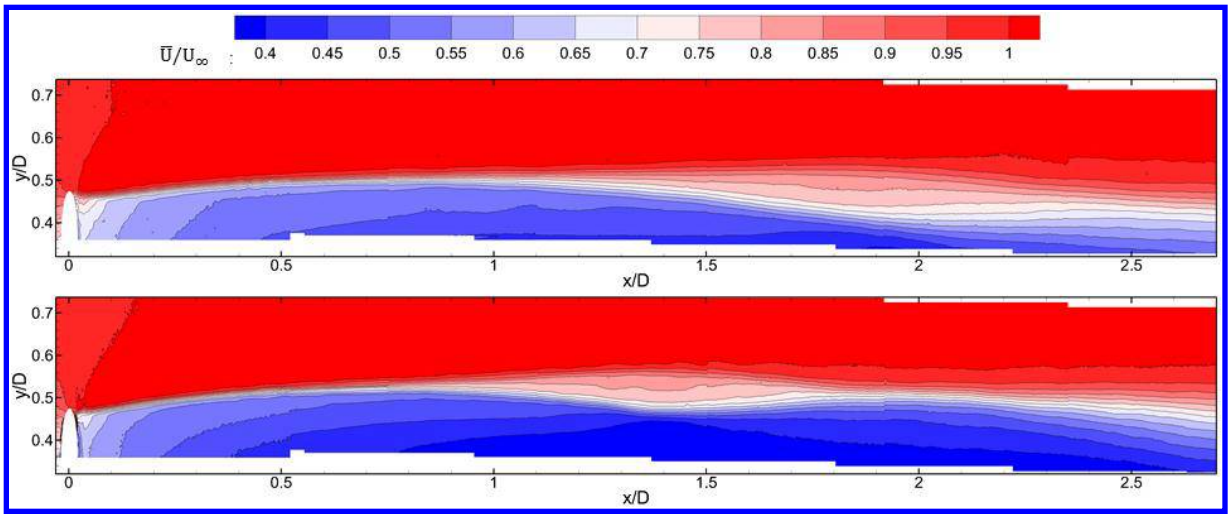

Figure 2 Normalized unconditioned average axial velocity of combined PIV fields in the wind-turbine wake, blade axis at P(x/D, y/D)=[0,0], λ = 4.8 (a) λ = 6 (b).

The flow associated with the raising of the leapfrogging instability is shown as contours of phase-locked average velocity in Figure 4 and Figure 3. The stream-line pattern is referenced to an observer travelling with the vortex convective velocity which is estimated from the phase-locked fields. Consequently, the vector fields and the stream-line pattern are representative of the 2-dimensional velocity field $[\bar{u} + \tilde{u} - U_c], [\bar{v} + \tilde{v}]$. It should be noted that this is based on the assumption of null vertical convective velocity. The axial convection velocity uc is estimated at 3.7 m/s for $\lambda = 6$ and 1.7 m/s for $\lambda = 4.8$. The two close-ups of Figure 4 and Figure 3 show the pairwise organization of the vortices, with duplet structures separated by stream-line saddle points A1, B1, A2, B2. The two arrowed lines indicate the converging and diverging separatrices connecting the two consecutive vortices. The inclination of the diverging separatrices with respect to the wake centre-line varies along the wake evolution due to the wake expansion and by the presence of the vortex instability. The value of the separatrix inclination with respect to the duplets middle plane was estimated to be about 40° in good agreement with the findings of Ref. 2.

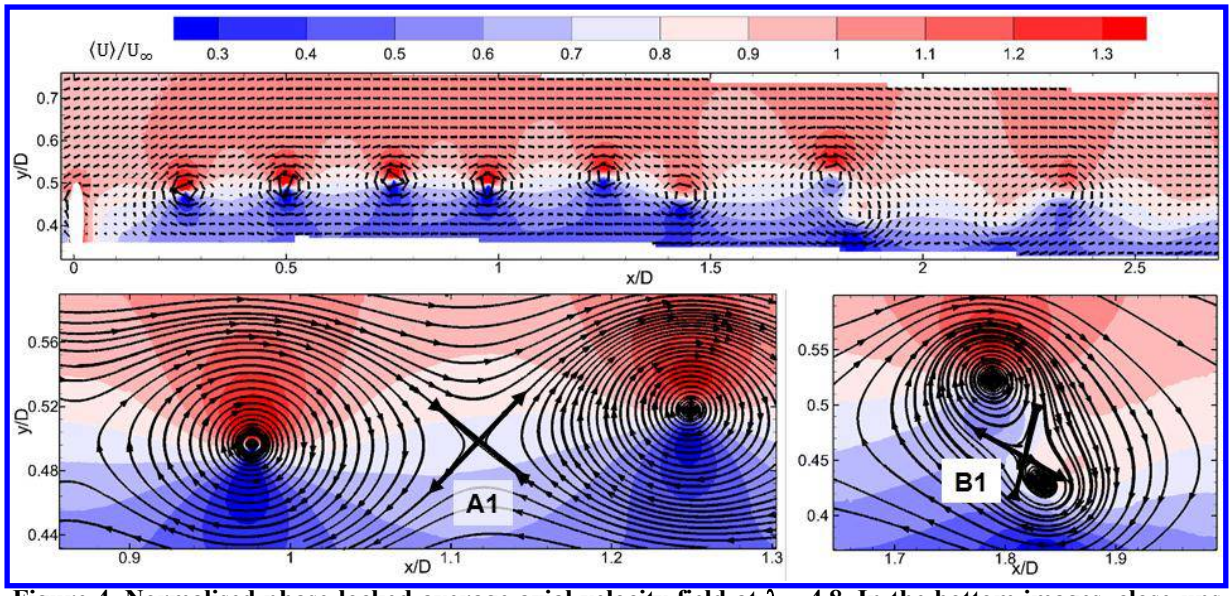

Figure 4. Normalised phase-locked average axial velocity field at λ = 4.8. In the bottom images, close-ups on the tip-vortices before and during leapfrogging

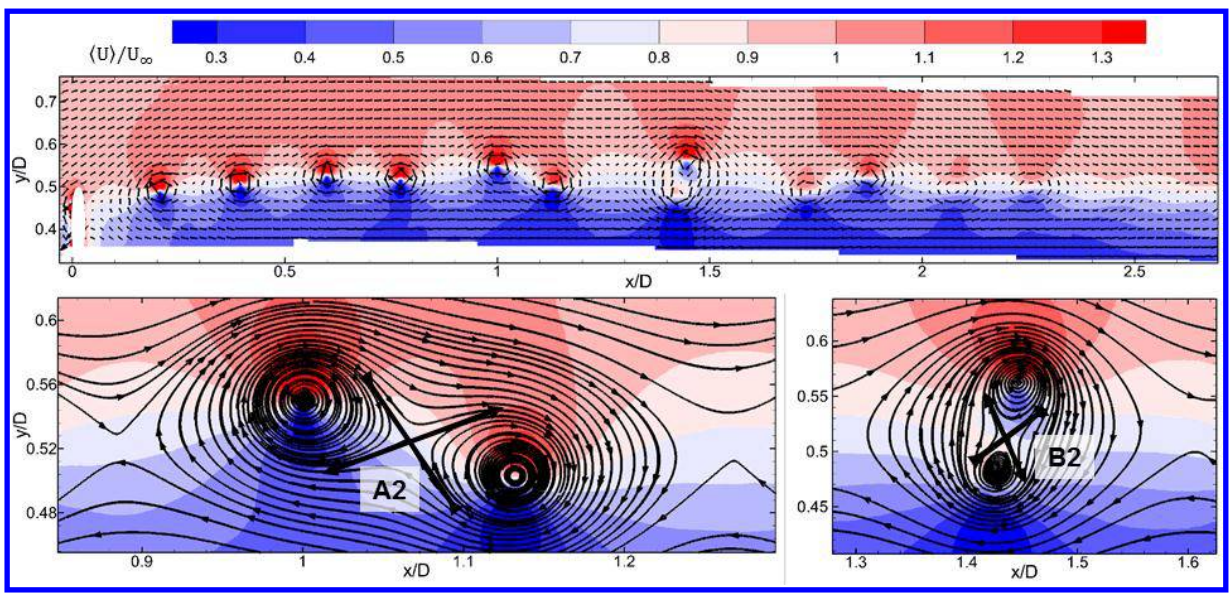

Figure 3. Normalised Phase-locked average axial velocity field at λ = 6. In the bottom images, close-ups on the tip-vortices before and during leapfrogging.

D. Turbulence intensity, mean flow kinetic energy transport and turbulence production

- **Turbulence intensity**

Ref. 17 have shown that the kinetic energy content of the wake starts increasing after the tip-vortex have paired and completed a 90° rotation around their saddle points. This location coincides with the onset of a more efficient wake mixing. However, it is still unclear what the role of the vortical structures is in the transport of the mean flow kinetic energy and in turn to the wake re-energising. To this purpose, the total turbulence intensity contours are firstly obtained from the unconditioned PIV measurements as:

$$TI = \frac{\overline{u_{RMS}}}{U_\infty} = \frac{1}{U_\infty}\sqrt{\frac{1}{3}\sum_{i=1}^{3}\overline{u'_i u'_i}} \tag{8}$$

and shown in Figure 5. In wind energy jargon, this is normally called the "added turbulence" and represents the flow turbulence caused by the presence of the turbine, which is added to the ambient turbulence [7]. This includes both the periodic and the random velocity fluctuations, which are not separated in a classical double Reynolds decomposition, as shown in Eq. (8). Coherent periodic structures as the tip-vortices are therefore accounted for as turbulence and this leads to the well-known peaks of turbulence intensity close to the rotor at the blade tip location, as also evident in Figure 5. However this is not theoretically right. In fact, as very well-expressed by Ref. 34, a vortex structure can be defined as a concentrated, continuous, coherent distribution of vorticity which is uniform in the direction of the vorticity vector and which grows in scale by viscous diffusion alone, whereas turbulence eddies may be described as vorticity-containing region of fluid. In this section, the contrasting roles in the transport of kinetic energy of this different flow structures will be shown. In order to isolate the contribution of the random fluctuations in a selected phase, the formulation in Eq. (9) is used to calculate the phase-locked average turbulence intensity, shown in Figure 6.

$$TI(\varphi) = \frac{\langle u_{RMS}\rangle}{U_\infty} = \frac{1}{U_\infty}\sqrt{\frac{1}{3}\sum_{i=1}^{3}\langle u_{s,i}u_{s,i}\rangle} \tag{9}$$

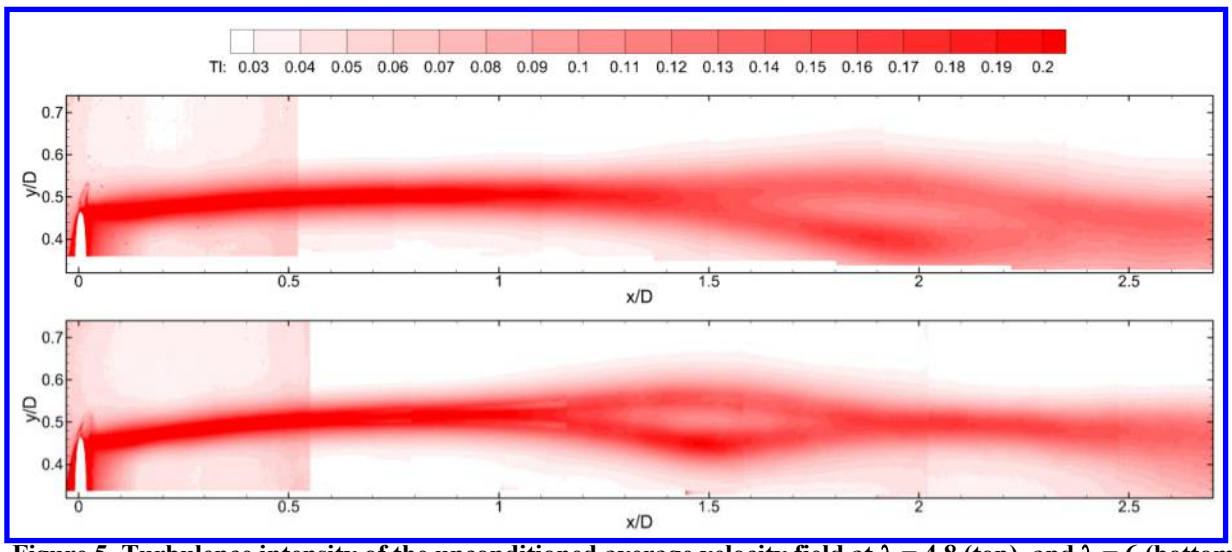

Figure 5. Turbulence intensity of the unconditioned average velocity field at λ = 4.8 (top), and λ = 6 (bottom).

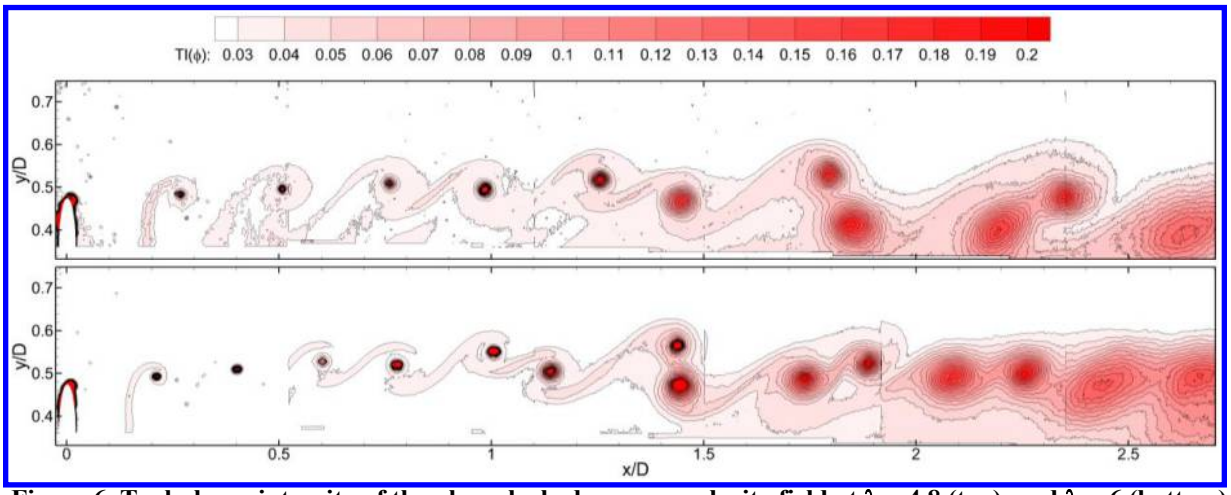

Figure 6. Turbulence intensity of the phase-locked average velocity field at λ = 4.8 (top), and λ = 6 (bottom).

A strong increase in the level of the turbulence intensity in the shear layer is shown after the location where the vortices have completed a 90° rotation. After this location, the turbulent mixing in the far-wake field is dominated by random fluctuations, determined by the breakdown and dissipation of the strong concentrated periodic fluctuations of the vortex system in the very near wake.

- **Mean flow kinetic energy fluxes**

The behaviour of the periodic vortical structures and the random turbulent fluctuations is studied via the calculation of the fluxes of the mean-flow kinetic energy. This can be done by estimating the terms contained in the gradient of the last element of Eq. (7), namely $-\overline{u}_i\left(\widetilde{u}_i\widetilde{u}_j\right)$ and $-\overline{u}_i\langle u_{s,i}u_{s,j}\rangle$. These terms represent the fluxes of the mean flow kinetic energy in a selected phase by action of the periodic (Figure 7) and random fluctuations (Figure 8) respectively. The spatial gradients of these terms represent therefore a net transport of kinetic energy in the volume of flow. The only terms which are supposed to contribute to the wind-turbine wake re-energising process are the fluxes of kinetic energy relative to the mean axial velocity directed toward the wake centreline, namely $\widetilde{\Phi} = -\overline{u}(\tilde{u}\tilde{v})$ and $\Phi_s = -\overline{u}\langle u_s v_s\rangle$ in the *x-y* plane of the measurements. Positive values mean downward fluxes of kinetic energy, therefore energy entrained in the inner part of the wake. Two zones can be identified. The first zone, before the vortex breakdown where the wake expansion occurs, shows the tip-vortices structures to be the only structures determining a mean flow kinetic energy transport across the wake layer, although with a negligible net value, due to both positive and negative contribution of similar magnitude.

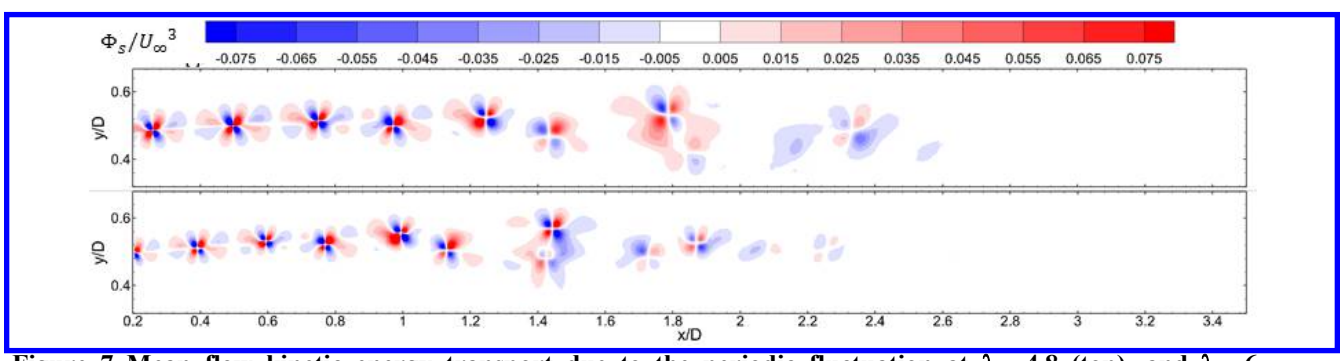

Figure 7 Mean flow kinetic energy transport due to the periodic fluctuation at λ = 4.8 (top), and λ = 6 (bottom).

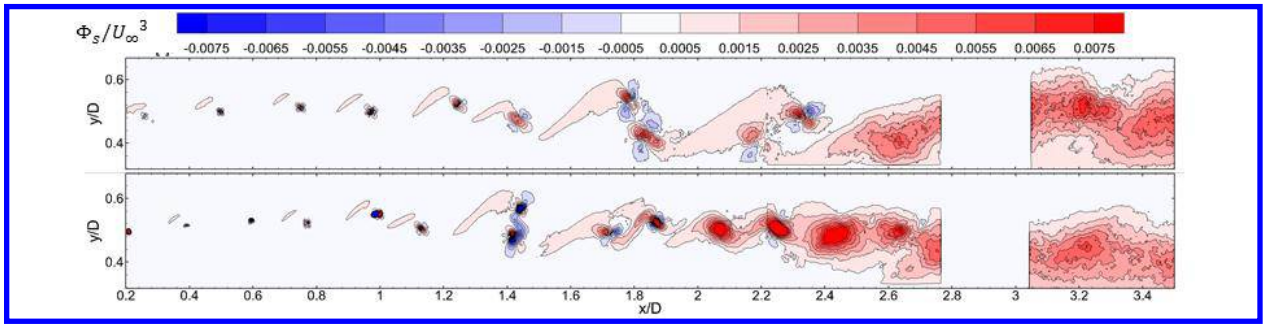

Figure 8 Mean flow kinetic energy transport due to the random fluctuations, at λ = 4.8 (top), and λ = 6 (bottom).

The second zone, after the wake instability and the tip vortex breakdown, is characterised by a downward net entrainment of kinetic energy, i.e. towards the inner region of the wake, caused by the random turbulent motions, signifying a dominant role of these flow structures in the re-energising process. The result is in accordance with the hypothesis of Ref. 18 who stated that the near wake tip-vortices are acting as a shield inhibiting the wake to mix with the outer flow.

- **Production of turbulent kinetic energy**

The phase-locked average production $\langle Pe \rangle$ of turbulent kinetic energy associated to random fluctuations, as presented in Ref. 6 is:

$$\langle Pe \rangle = -\langle {u_s}^2 \rangle \frac{\partial \langle u \rangle}{\partial x} - \langle {v_s}^2 \rangle \frac{\partial \langle v \rangle}{\partial y} - \langle u_s v_s \rangle \left(\frac{\partial \langle u \rangle}{\partial y} + \frac{\partial \langle v \rangle}{\partial x} \right) \tag{10}$$

This term constitute a sink for the phase average flow kinetic energy and can as such be considered as destruction of kinetic energy of the phase-locked average velocity field. The studies in Ref. 2 and Ref. 6 show that the saddle points between two consecutive vortices are zones of large production of turbulent kinetic energy: in fact, the turbulence is produced mainly in the braids between the large vortices along the divergent separatrix, as noted by Ref. 11, and then transported to and accumulated in the vortices. Figure 9 shows how the contours of $\langle Pe \rangle$ are crowded in the region along the diverging separatrix, in accordance with abovementioned studies. The production of turbulence values along the separatrix for both tip-speed ratios reach their extrema in the leapfrogging location. It must be noted that the strong peaks of turbulence production in correspondence of the vortex cores are due to phase fluctuation of the vortex structure itself (vortex wandering in Ref. 8) and to the high values of experimental noise in those regions.

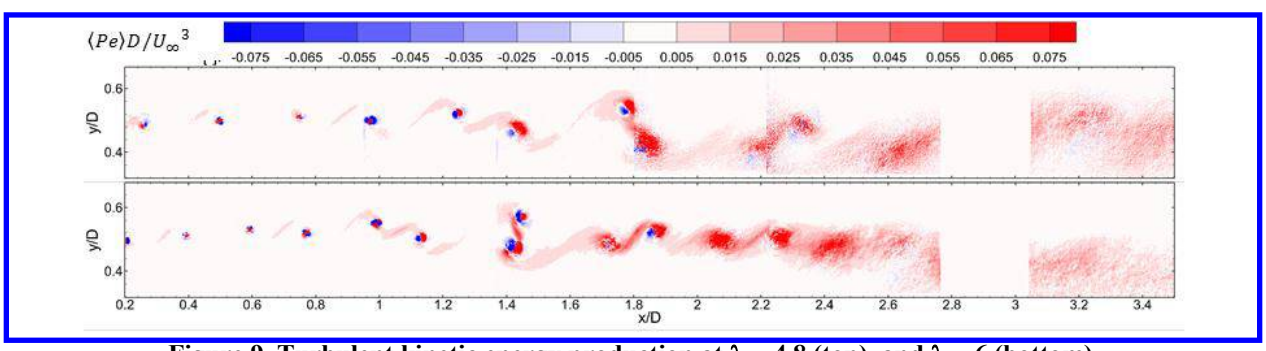

Figure 9. Turbulent kinetic energy production at λ = 4.8 (top), and λ = 6 (bottom).

IV. Conclusions

An experimental investigation has been performed using stereo particle image velocimetry in order to study the evolution of the vortex structure in the wake of a 0.6 m diameter horizontal axis wind turbine and the influence of the pairwise instability of the tip-vortex filaments (the so-called leapfrogging phenomenon) on the evolution of the far wake turbulence and mean flow kinetic energy transport. Observation of the unconditioned average velocity field demonstrated a localised increase of the wake shear layer thickness in correspondence of the wake instability, which also coincides with the location of its maximum. A detailed analysis of the interacting vortex doublets show a general structure in agreement with previous studies on bluff body wakes and planar jets, with converging/diverging separatrices intersecting in saddle points which constitute peaks of turbulence production. The analysis of the flow statistics revealed a major difference between the unconditioned average and the phase-locked average turbulence intensity. The former one exhibits characteristic peaks close to the rotor at the blade tip region due to the presence of strong coherent vortices; the latter one shows a sudden increase after the tip-vortex breakdown. The investigation of the mean flow kinetic energy transport demonstrates a deeply different nature of the vortex structures and the turbulent fluctuations, which normally are both accounted for as turbulence. In particular the analysis suggests the presence of three zones characterised by a totally different mixing. In the first zone the vortices inhibit the mixing of the wake during its expansion, in the transition zone the leapfrogging causes a sudden increase of the net entrainment of the mean flow kinetic energy and in the third zone a more efficient mixing contributes to the wake re-energising, in accordance with previous work from the authors [17]. This research explains the dominant effect that the wake instability has on the wake mixing, already expressed in a qualitative way by previous literature.

References

[1] Antonia, R. A. and Browne, L. W. B. 1987 Quadrant analysis in the turbulent far-wake of a cylinder. *Fluid Dynamics Research* 2(1), 3.

[2] Antonia, R. A., Browne, L. W. B., Bisset, D. K. and Fulachier, L. 1987 A description of the organized motion in the turbulent far wake of a cylinder at low Reynolds number. *Journal of Fluid Mechanics* 184, 423-444.

[3] Antonia, R. A., Chambers, A. J., Britz, D. and Browne, L. W. B. 1986 Organized structures in a turbulent plane jet: topology and contribution to momentum and heat transport. *Journal of Fluid Mechanics* 172, 211-229.

[4] Barthelmie, R. J., Rathmann, O., Frandsen, S. T., Hansen, K. S., Politis, E., Prospathopoulos, J., Rados, K., Cabezón, D., Schlez, W., Phillips, J., Neubert, A., Schepers, J. G. and Van Der Pijl, S. P. 2007 Modelling and measurements of wakes in large wind farms. *Journal of Physics: Conference Series* 75(1), 012049.

[5] Browand, F. K. and Weidman, P. D. 1976 Large scales in the developing mixing layer. *Journal of Fluid Mechanics* 76(01), 127-144.

[6] Cantwell, B. and Coles, D. 1983 An experimental study of entrainment and transport in the turbulent near wake of a circular cylinder. *Journal of Fluid Mechanics* 136, 321-374.

[7] Crespo, A., Hernández, J. and Frandsen, S. 1999 Survey of modelling methods for wind turbine wakes and wind farms. *WIND ENERGY* 2(1), 1-24.

[8] Dobrev, I., Maalouf, B., Troldborg, N. and Massouh, F. 2008 Investigation of the Wind Turbine Vortex Structure. 14th International Symposium on Applications of Laser Techniques to Fluid Mechanics. Lisbon, Portugal.

[9] Escudié, R. and Liné, A. 2003 Experimental analysis of hydrodynamics in a radially agitated tank. *AIChE Journal* 49(3), 585-603.

[10] Felli, M., Camussi, R. and Di Felice, F. 2011 Mechanisms of evolution of the propeller wake in the transition and far fields. *Journal of Fluid Mechanics* 682, 5-53.

[11] Hussain, A. K. M. F. 1981 Role of coherent structures in turbulent shear flows. *Proceedings of the Indian Academy of Sciences Section C: Engineering Sciences* 4(2), 129-175.

[12] Hütter, U. 1977 Optimum Wind-Energy Conversion Systems. *Annual Review of Fluid Mechanics* 9, 399-419.

[13] Ivanell, S. 2009 Numerical Computations of Wind Turbine Wakes. Linn´e Flow Centre, Department of Mechanics. SE-100 44 Stockholm, Sweden, Royal Institute of Technology KTH - Gotland University.

[14] Ivanell, S., Mikkelsen, R., Sørensen, J. N. and Henningson, D. 2010 Stability analysis of the tip vortices of a wind turbine. *WIND ENERGY* 13(8), 705-715.

Joukowsky, N. E. 1912 Vortex Theory of Screw Propeller. Paris, Gauthier-Villars.

[16] Leishman, J. G. 1998 Measurements of the aperiodic wake of a hovering rotor. *Experiments in Fluids* 25(4), 352-361.

[17] Lignarolo, L. E. M., Ragni, D., Krishnaswami, C., Chen, Q., Simao Ferreira, C. J. and Van Bussel, G. J. W. 2013 Experimental analysis of the wake of a horizontal-axis wind-turbine model. *Renewable Energy*, (under peer review).

[18] Medici, D. 2005 Experimental Studies of Wind Turbine Wakes – Power Optimisation and Meandering. Mechanics. Stockholm, Royal Institute of Technology (KTH).

[19] Okulov, V. and Sorensen, J. 2004 Instability of a vortex wake behind wind turbines. *Doklady Physics* 49(12), 772-777.

[20] Okulov, V. L. 2004 On the stability of multiple helical vortices. *Journal of Fluid Mechanics* 521, 319-342.

[21] Okulov, V. L. and Sorensen, J. N. 2007 Stability of helical tip vortices in a rotor far wake. *Journal of Fluid Mechanics* 576, 1–25.
Raffel, M., Willert, C. E., Wereley, S. and Kompenhans, J. 2007 Particle Image Velocimetry: A Practical Guide.
[23] Reynolds, W. C. and Hussain, A. K. M. F. 1972 The mechanics of an organized wave in turbulent shear flow. Part 3. Theoretical models and comparisons with experiments. *Journal of Fluid Mechanics* 54(02), 263-288.
[24] Schepers, J. G. 2012 Engineering models in wind energy aerodynamics. Aerospace Engineering, Delft University of Technology. PhD.
[25] Schreck, S., Lundquist, J. and Shaw, W. 2008 U.S. Department of Energy workshop report research needs for wind resource characterization. Golden, CO :, National Renewable Energy Laboratory.
Selig, M. S., Guglielmo, J. J., Broeren, A. P. and Giguère, P. 1995 Summary of Low-Speed Airfoil Data. Virginia Beach, VA, SoarTech Publications.
[27] Snel, H., Schepers, J. G. and Montgomerie, B. 2007 The MEXICO project (Model Experiments in Controlled Conditions): The database and first results of data processing and interpretation. *Journal of Physics: Conference Series* 75(1), 012014.
[28] Sorensen, J. N. 2011 Instability of helical tip vortices in rotor wakes. *Journal of Fluid Mechanics* 682, 1-4.
[29] Vermeer, L. J., Sørensen, J. N. and Crespo, A. 2003 Wind turbine wake aerodynamics. *Progress in Aerospace Sciences* 39(6-7), 467-510.
[30] Whale, J., Anderson, C. G., Bareiss, R. and Wagner, S. 2000 An experimental and numerical study of the vortex structure in the wake of a wind turbine. *Journal of Wind Engineering and Industrial Aerodynamics* 84(1), 1-21.
[31] Widnall, S. E. 1972 The stability of a helical vortex filament. *Journal of Fluid Mechanics* 54(04), 641-663.
[32] Winant, C. D. and Browand, F. K. 1974 Vortex pairing : the mechanism of turbulent mixing-layer growth at moderate Reynolds number. *Journal of Fluid Mechanics* 63(02), 237-255.
[33] Wu, Y.-T. and Porté-Agel, F. 2011 Large-Eddy Simulation of Wind-Turbine Wakes: Evaluation of Turbine Parametrisations. *Boundary-Layer Meteorology* 138(3), 345-366.
[34] Yule, A. J. 1978 Large-scale structure in the mixing layer of a round jet. *Journal of Fluid Mechanics* 89(03), 413-432.